Journal of the European Ceramic Society **18** (1998) 1593–1598

PII: S0955-2219(98)00072-7
0955-2219/98/$—see front matter

Characterisation of the Surface Conductivity of Glassy Materials by Means of Impedance Spectroscopy Measurements

Claudio Fontanesi,* Cristina Leonelli, Tiziano Manfredini, Cristina Siligardi and Gian Carlo Pellacani

Department of Chemistry, University of Modena, Via Campi 183, 41100 Modena, Italy

(Received 28 July 1997; accepted 16 February 1998)

Abstract

Abstract The phenomenon of tin dioxide doping by antimony, Sb(V), atoms in semiconductive glazes is discussed. In particular, the impedance spectra of the glaze surface at room temperature were experimentally determined, and the results were analysed in terms of equivalent circuits. The parameters resulting from the fitting procedure were related to the SnO_2/Sb(V) relative content, the SnO_2/Sb (V) percentage in the glaze, and the microstructure as observed by SEM. It is proposed that the addition of SnO_2 and Sb_2O_3 to a common glaze for ceramic tile results in a semiconductive continuous phase, whose electrical characteristics fulfil the antistatic floor regulation, as far as surface conductivity is concerned. As a whole the obtained results suggest that the thermal cycle used in fast firing technology is capable to promote the oxidation of Sb_2O_3 to Sb_2O_4, resulting in a sufficient amount of Sb(V) capable of generating a semiconductive behaviour of the SnO_2 crystalline phase dispersed in the glaze. © *1998 Elsevier Science Limited. All rights reserved*

1 Introduction

SnO_2 is a broad band semiconductor in which *s* and *p* electrons propagate with large mobility.[1] As calculated by Roberston,[2] the valence band is mainly composed of O_{2p} orbitals and the conduction band consists of Sn_{5s}, and Sn_{6s}, orbitals. The intrinsic energy gap can be as large as 3·6 eV thus making stoichiometric SnO_2 a poor conductor at room temperature. The high conductivity seen and measured occurs when there is a deviation from stoichiometry by the introduction of dopants.

It is of interest the determine the dopant. In the case of SnO_2 an oxygen vacancy on the interstitial Sn can be the donor site, it can be used as a film for transparent electrode or as a gas sensor (O_2, H_2, CO, C_3H_8).[3,4] The dopant can be an 'impurity', an atom different from Sn or O which can be either donor or acceptor type. Sb(V) is a typical donor for Sn(IV), for it donates an electron to the conduction band.[5] These electrons can then participate in transport processes (while the impurity centres become positively charged). Donors give rise to electronic type or n-type of conductivity in semiconductors.

The field of oxide-conductive amorphous materials is indeed of large interest, both as far as the conduction mechanism is concerned and the application of easy forming high quality semiconductors. Semiconducting glasses doped with SnO_2 and Sb_2O_5 have been the object of very few scientific papers in the English literature.[6–10] On the contrary the use of SnO_2-glasses or glazes has been very large in the past as grey-blue pigment and as semiconductor. As witnessed by a good number of patents.[11–13]

In the last few years, some experimental reports appeared on the doping of SnO_2 by Sb_2O_3 as starting material when used as glass coatings.[14] The low cost and easy availability of such an oxide make it an interesting material in the industrial use as precursor for Sb(V). These characteristics, accompanied by the thermal stability of the two oxides ($T_{decomposition} > 1100°C$), can be exploited for preparing silicate glasses characterised by production temperatures ranging between 700 to 1200°C, and featuring a semiconductive electrical behaviour. Applications for such semiconductive

*To whom correspondence should be addressed.
E-mail: fontanes@unimo.it

silicate glasses are ceramic coatings, in particular glazes for tiles used for antistatic floor covering.[14]

The aim of this paper is manifold: (a) to obtain glassy coatings, based upon semiconductive SnO_2/Sb(V) mixture, for ceramic tiles which satisfy Italian law for antistatic floor; (b) to use Sb_2O_3 as precursor for Sb(V), and (c) to reduce and/or eliminate prefiring of the SnO_2/Sb_2O_3 mixture in order to match with the single fast firing schedule applied in industrial tile production. The literature does not report any attempts made in the direction of point (c). The glaze formulations considered in this work were subsequently studied in order to validate a microstructural conduction model hypothesised for similar conductive materials.[15]

2 Experimental Procedure

2.1 Materials

The amorphous matrix of the glaze was based on a glaze formulation commonly used in fast firing technology (Table 1), which was added to different SnO_2/Sb_2O_3 mixtures as detailed in the following.

A first set of samples was obtained by adding 35 g of SnO_2/Sb_2O_3 mixtures, of various reciprocal percentage, to 65 g of traditional glaze (Table 2). Then, the tin to antimony oxide ratio was kept constant ($SnO_2/Sb_2O_3 = 33/2$), whilst varying the composition with respect to the traditional composition glaze (Table 3).

The glazed body was fired industrially at approximately 1100°C during a 50 min heating cycle.

2.2 Characterisation

The as-fired glaze surface was investigated after metal coating by scanning electron microscopy, SEM (Philips XL-40) provided with a backscattered electrons, BSE, detector and a X-ray fluorescence energy dispersion spectrometry, EDS, detector (EDAX PV9900) as well.

Aiming to characterise the surface impedance of the glassy glaze, a dedicated electrode design was set up by the authors: two conductive carbon stripes parallel with respect to each other were deposited on the glaze surface; each rectangular stripe was 10 mm wide × 20 mm long, with a reciprocal separation distance of 10 mm. Carbon glue was used to actuate the electrical connection between the two carbon stripes and the measuring devices. Impedance spectra were recorded at room temperature in the 65 kHz to 1 Hz range, with a 0·5 V alternating current peak-to-peak amplitude, using a frequency response analyser (Solartron 1250) and an electrochemical interface (in the two electrode configuration) (Solartron 1286, output impedance $\geq$ 10 GΩ), which was set to 0 d.c. potential with the only task to optimise the resistive load seen by the frequency response analyser. The electrochemical apparatus was automatically controlled (IBM PS/2 Mod. 30) through a General Purpose Interface Bus (GPIB) port via an originally implemented program. Subsequent impedance data analysis was performed by using the complex non-linear least squares immittance fitting procedure as implemented in the LOMFP package.[16]

Table 1. Traditional glaze composition

	SiO_2	B_2O_3	ZnO	BaO	CaO
(wt%)	23	20	28	22	7

Table 2. Global glaze composition, varying the tin to antimony oxide ratio

Glaze number	*I*	*II*	*III*	*IV*	*V*
Traditional glaze (wt%)	65	65	65	65	65
SnO_2 (wt%)	34·5	34	33·5	33	32·5
Sb_2O_3 (wt %)	0·5	1	1·5	2	2·5

Table 3. Global glaze composition, with constant tin to antimony oxide ratio

Glaze number	*VI*	*VII*	*VIII*
Traditional glaze (wt%)	55	75	85
($SnO_2/Sb_2O_3 = 33/2$)	45	25	15

3 Results and Discussion

3.1 Microstructure determination

The as-fired surface of the different glaze formulations present similar features, [Fig. 1(a)], at the scanning electron microscopy observation. Bright areas in which are visible 0·5÷1 μm crystals are homogeneously distributed all over the surface. As from EDS analyses and X-ray diffraction the crystals appeared to be SnO_2 with the cassiterite structure.[17]

The backscattered electron, BSE, micrograph [Fig. 1(b)] shows that the crystals are embedded in an amorphous phase. Since the brightness of such a BSE image is directly correlated to the atomic weight of the phase components, it can be stated that the amorphous phase is not uniform, being the crystals surrounded by tin-rich areas which provide a continuous network (this will be shown to be consistent with conductivity results). Such a result, has been confirmed by the X-ray fluorescence map of Sn atoms [Fig. 1(c)], where the distribution of tin atoms borders the crystalline areas. For sake of comparison the Si atom distribution is reported in Fig. 1(d), showing a silicon-free areas corresponding to tin-rich glass. Overlapping the crystalline

areas as from BSE image to the Sn map, a picture reproducing the microstructural model proposed by Nakamura *et al.* in the 1980s is obtained (Fig. 2(b)].

The SEM outcome can be considered as an experimental validation of such a model, in which cassiterite doped crystals are interconnected by Sn-rich glaze.[14] The microstructural model is based upon two main considerations: the retention of cassiterite structure by tin dioxide, and the presence of Sb(V) in the SnO_2 crystalline matrix. The first point is assured by the well-known phenomenon of partial dissolution of SnO_2 in glasses, so that tin dioxide has been used in the past as glass opacifier, as well as a nucleating agent. For this reason it may be reasonable to suppose that the tin-rich glaze is cassiterite-rich glaze, in the sense that Sn atoms do not actually enter the glass structure, responsible for the semiconduction process and the continuity of the semiconductive phase. The second requirement is realised by tile oxidation of Sb_2O_3 to either Sb_2O_4 or Sb_2O_5, as a result of the firing treatment at 1100°C, temperature at which the volatilisation of the antimony compounds is evidently not complete. The distribution of Sb atoms does not present any particular feature, probably due to its low percentage in the glaze formulation; anyway its doping effect on tin oxide crystals is experimental evidence (see next paragraph).

3.1.1 Impedance measurements

Figures 3–5 show impedance spectra which are representative of all the different experimental behaviour exhibited by samples I to VIII.

In fact, impedance measurements yield three different types of spectra, all of them are evidently distorted and depressed arcs with respect to the real axis, Figs 3–5 (referring to the IV, VI and VII glaze samples respectively).

The spectra of Figs 3 and 4 can be interpreted on the basis of the same equivalent circuit, a cell constituted by a resistance R_2 in parallel with a distributed constant time element altogether in series with a resistor R_1, (Fig. 6).

Actually, for the impedance spectrum in Fig. 3 the high frequency range is lacking; likely an intersection, on the z_R axis, similar to that shown in

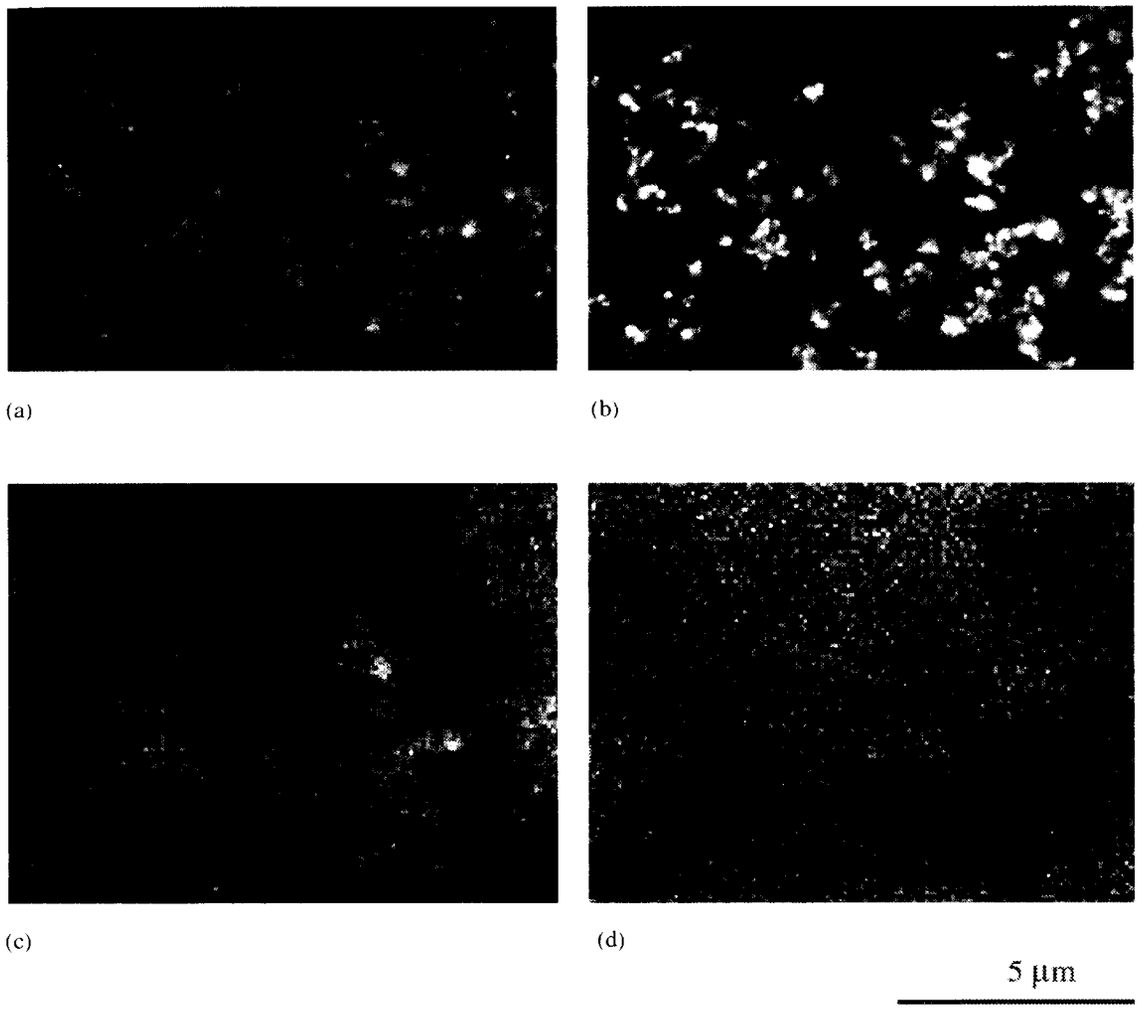

Fig. 1. SEM micrographs of (a) secondary electron image; (b) backscattered electron image; (c) distribution of Sn atoms and (d) of Si atoms.

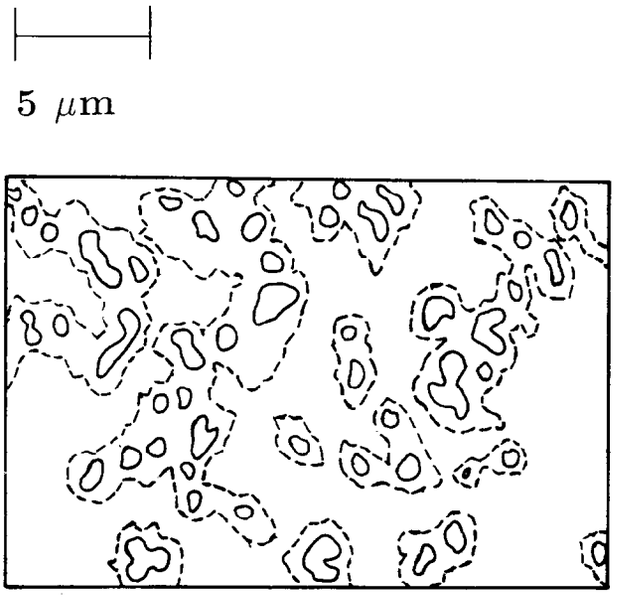

Fig. 2. Model of semiconductive SnO_2/Sb_2O_3 glaze. Continuous lines enclose areas proper of the SnO_2 crystalline phase [Fig. 1(b)]. The area enclosed between the dotted and continuous lines is due to the partially dissolved SnO_2 phase into the amorphous glaze [Fig. 1(c)].

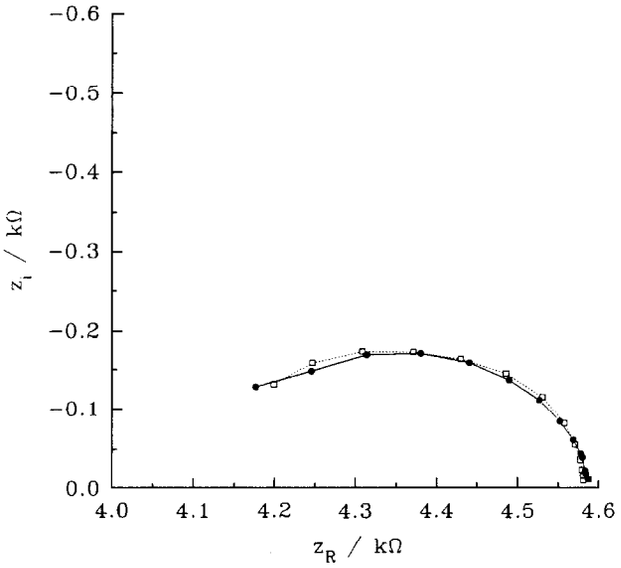

Fig. 3. Impedance spectrum of sample IV: (●) experimental points; (□) points following DAE fitting.

Fig. 4 would have been obtained at higher frequencies.

Thus, the impedance spectra of samples I to VII were fitted simulating the impedance of the distributed constant time element as a generalised finite Warburg (GFW) element.[18]

$$Z_{GFW} = R \times tanh\left[(iTw)^{\phi}\right]/(iTw)^{\phi}$$

and exponential distribution of activation energies (DAE)[19]

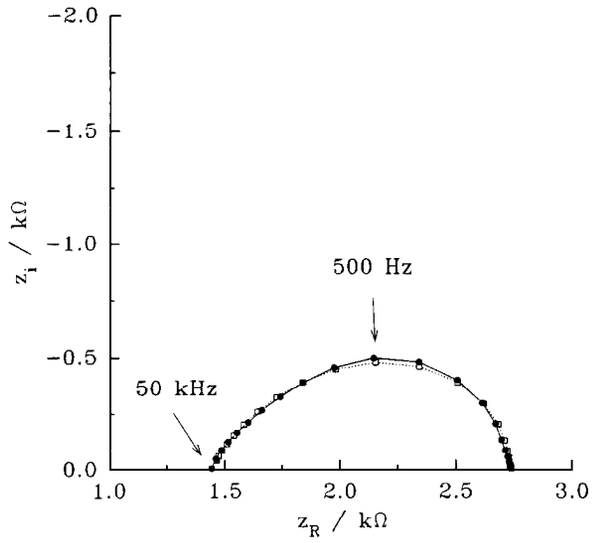

Fig. 4. Impedance spectrum of sample VI: (●) experimental points; (□) points following DAE fitting.

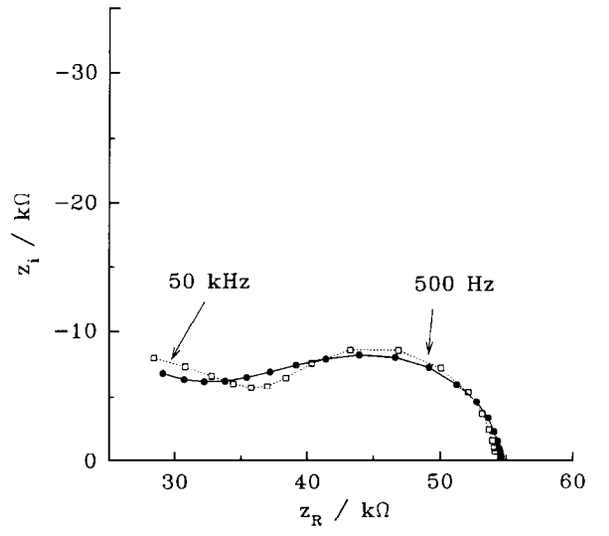

Fig. 5. Impedance spectrum of sample VIII: (●) experimental points; (□) points following DAE fitting.

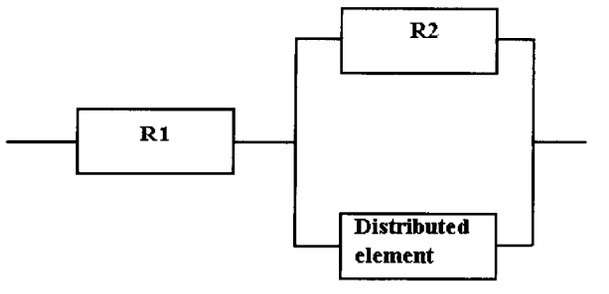

Fig. 6. Equivalent circuit representative of the electrical behaviour of the I to VII glaze samples.

$$Z_{DAE} = \frac{\phi}{(r^{\phi} - 1)} 1 \int_{1}^{r} \frac{W^{(\phi-1)}}{(1 + isW)} dW$$

where, $i = (-1)^{1/2}$, R is the d.c. resistance associated with the distributed element, T the corresponding time constant, $w = 2\pi f$ depends on the

frequency (f) of the a.c. signal used as a probe, ϕ is an adjustable parameter which is a function of the exponential thermal activation of the resistance and capacity (because both GFW and DAE models assume that the resistance and capacity values depend on the temperature through an exponential law), $s = w\,\tau_0$(τ_0 is the zero frequency limit of the distributed element time constant), $W = w\,\mathrm{R}\,\mathrm{C}$ and, eventually, $r = W_\infty$ (is the W value in the limit of infinite frequency).[19]

The impedance spectrum of the sample VIII shows the existence of a second arc in the high frequency range (Fig. 5), the experimental data can be effectively fitted using the same equivalent circuit set out in Fig. 6, but with the addition of a capacity in parallel to R_1.

Note that, in all the examined cases the imaginary part of the impedance, z_i, tends to zero for frequencies lower than 70 Hz, samples I to VIII represented by Figs 3–5.

In fact, the d.c. resistance values determined by using an ohm meter and the low frequency module of the impedance (which virtually coincides with z_R, because $|z| = (z_R + z_i)^{1/2}$; $Hz \to 0$, $z_i \to 0$ implying $|z| \to z_R$) are virtually identical.

As a whole, these results suggest that the conduction process is elcctronic in nature. This outcome is in agreement with other studies relating to the study of impedance spectra of semiconductors.[20]

The results of the fitting procedure are set out in Tables 4 and 5. Note that, the two models, GFW and DAE, provide quite similar values for R_1, R_2 and τ_2.

The R_1 values (i.e. the high frequency limit of the impedance) is associated to the actual surface bulk resistance of the material, while the τ_2 and R_2 components of the arc impedance are representative of the inter-grain (or the interface between different phases) resistance and capacity.[21] It can be seen that linear relationships are obtained plotting both GFW and DAE R_2 values as a function of the SnO_2 as well as the Sb_2O_3 percentage, compare Tables 2–5. A similar result is yielded by plotting $R_1 + R_2$ (Tables 4 and 5) as a function of

Table 4. CNLS fit using the generalized finite Warburg model

Sample	*φGFW*	R_2/Ω	$\tau_2 \times 10^5$/s	R_1/Ω	*Capacity*[a]*/F*
I	0·45	1950	2·23	6710	
II	0·42	1220	2·21	4780	
III	0·45	972	2·25	3180	
IV	0·40	578	3·48	4014	
V	0·40	403	1·82	2760	
VI	0·48	1330	88·2	1390	
VII	0·45	3130	3·41	6640	
VIII	0·30	39500	0·601	14700	1·190

[a]In parallel with R_1.

Table 5. CNLS fit using the distributed activation energy model

Sample	r	*φDAE*	R_2/Ω	$\tau_2 \times 10^5$/s	R_1/Ω	*Capacity*[a]*/F*
I	90	0·85	1800	1·80	6840	
II	90	0·55	1210	1·21	4780	
III	50	0·55	1030	2·16	3110	
IV	1000	0·45	583	4·07	4005	
V	2·0	0·20	306	1·73	2860	
VI	5·5	0·75	1283	78·1	1450	
VII	4·5	0·60	2990	3·2	6760	
VIII	5·0	0·60	34600	0·29	18900	6·88

[a]In parallel with R_1.

both the SnO_2/Sb_2O_3 oxide ratio (samples I–V, Table 2) and with respect to the fixed SnO_2/Sb_2O_3 total content (samples IV, VI, VII).

These results suggest that the phase formed by the SnO_2 is coherently dispersed in the glass matrix constituting a continuous network, so to allow the motion of electrons through the material.

The glaze VIII represents the only exception, featuring the presence of a second high frequency arc. This result seems to be indicative of a different morphology in the oxide network, probably in this case the oxide mixture results incoherently totally dissolved within the glassy matrix.

To give a more sound basis to the hypothesis of an electronic in nature conduction process, the d.c. resistance of the sample IV was also measured as a function of the temperature in the range between 25 and 300°C. Figure 7 shows the relevant conductance, (G), versus (1/T) plot. The conductance is found to increase monotonically as a function of the temperature and an activation energy of

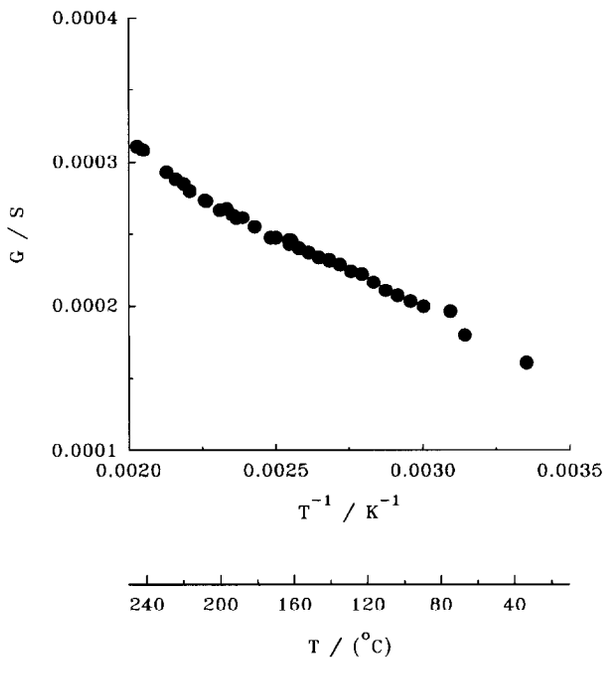

Fig. 7. Conductivity as a function of the inverse of the temperature, sample IV.

0·05 eV can be tentatively obtained by the nearly linear ln(G) versus (1/T) pattern, indicating the extrinsic semiconductive nature of the examined systems.

This finding is in line with the results shown in Ref. 22, even if in that study the semiconducting activity of SnO_2 ceramics was mainly related to the simultaneous presence of copper oxide in the specimen. Here is not clearly the case, the only doping compound present in the raw material is Sb_2O_3.

4 Conclusions

The SnO_2/Sb_2O_5 based glazes here studied show impedance spectra featuring depressed and not symmetric arcs. The 'generalised finite Warburg element'[18] and the 'exponential distribution of activation energies'[19] impedance models allowed an effective fit of the experimental data.

In all the examined cases, the impedance spectra exhibit a tendency to reach a purely resistive finite value in the low frequency limit ($z_i \rightarrow 0$). This finding, together with the results obtained by the analysis of the dependence of the conductance as a function of temperature (only for sample IV), suggests that the electronic conduction mechanism is responsible of the glaze surface conductivity.

Moreover, the relationships observed between the R_2 (as well as $R_1 + R_2$) values and the Sb_2O_3 content of the samples indicate that the antimony oxide is responsible of the semiconductivity observed for the materials here studied.

This overall picture is consistent with SEM micrographs and X-ray Sn map, which indicate the partial dissolution, within the glassy matrix of SnO_2, crystals, implying the formation of a continuous conductive oxide network.

References

1. Tsuda, N., Nasu, K., Yanase, A. and Siratori, K., *Electronic Conduction of Oxides*. Springer-Verlag, Berlin, 1983, pp. 116–123.
2. Robertson, L, Electronic structure of SnO_2, GeO_2, PbO_2, TeO_2 and MgF_2. *J. Phys. C: Solid State Phys.*, 1979, **12**, 4767–4776.
3. Samson, S. and Fonstad, C. G., Defect and electronic donor levels in stannic oxide crystals. *J. Appl. Phys.*, 1973, **44**, 4618.
4. Lee, J.-H. and Park, S.-L., Temperature dependence of electrical conductivity in polycrystalline tin oxide. *J. Am. Ceram. Soc.*, 1990, **73**, 2771–2774.
5. Shklovskii, B. L, and Efros, A. L., *Electronic Properties of Doped Semiconductors*, Springer Series in Solid-State Science, 45, Springer-Verlag, Berlin, 1984, pp. 2–254.
6. Goodman, J. F. and Gregg, S. L., Production of active solids by thermal decomposition XI. Heat treatment of precipitated stannic oxide. *J. Chem. Soc.*, 1960, **11**, 1162–1167.
7. Selmi, F. A. and Amarakoon, V. R. W., Grain boundary engineering of semiconducting tin oxide via sol-gel coating. *Ceram. Eng. Sci. Proc.*, 1987, **8**, 1120–1127.
8. Carturan, G., Giordano Orsini, P., Scardi, P. and Di Maggio, R., Effect of Sn/Sb ratio in determining crystallise size of SnO_2-Sb_2O_5 semiconductors. *J Mater. Sci.*, 1988, **23**, 3156–3160.
9. Powell, D. G., Semiconducting glazes for high voltage insulators. *Am. Ceram. Soc. Bull.*, 1973, **52**, 600–603.
10. Binns, D. B., Conducting-glazes. I. *Trans. Brit. Ceram. Soc.*, 1971, **70**, 253–263.
11. Philips Co. (Holland), British Patent No. 650.099, 1947.
12. Binns, D. B., British Ceramic Research, British Patent No. 982.600, 1970.
13. Bonfatti, L., Leonelli, C. and Settembre Blundo, D., Procedimento per la produzione di piastrelle antistatiche di grès porcellanato Italian Patent No. MI93A002448, 1993.
14. Nakarnura, M., Kinuta, K. and Shiomi, H., Semiconducting glaze using fine particles of SnO_2 doped with Sb_2O_5 by a mechano-chemical process. *Cer. Acta*, 1990, **2**, 57–65.
15. Nakarnura, M., Kamino, M., Nagano, T. and Arakawa, M., Microstructure and electrical properties of semiconducting tin oxide glaze. *Yogyo-Kyokai-Shi*, 1987, **95**, 562–566.
16. Macdonald, J. R., Complex Nonlinear Least Squares Immittance Fitting Program, LOMFP, package, Version 05130/1987.
17. Lonelli, C., Manfredini, T., Pellacani, G. C., Settembre Blundo, D., and Bonfatti, L., Esmalte de revestimientos ceramicos con caracteristicas semiconductoras para uso en lugar de concentracion de cargas estaticas. *Bol. Soc. Es. Ceram. y Vidrio*, in press.
18. Franceschetti, D. R. and Macdonald, J. R, Diffision of neutral, charged species under small signal a.c. conditions.. *J. Electroanal. Chem*, 1979, **101**, 307–311.
19. Macdonald, J. R., Frequency response of unified dielectric and conductive systems involving n exponential distribution of activation energies. *J. Appl. Phys.*, 1985, **58**, 1955–1970.
20. Macdonald, J. R., *Impedance Spectroscopy*, Wiley-Interscience, New York, 1987.
21. Bonanos, N. and Butler, E. P., Ionic conductivity of monoclinic and tetragonal Yttria-Zirconia single crystals. *J. Mat. Sci. Lett.*, 1985, **4**, 561–564.
22. Zuca, S., Terzi, M., Zaharescu, M. and Matiasovsky, K., Contribution to the study of SnO_2-based ceramics. *J. Mat. Sci.*, 1991, **26**, 1673–1676.